Co-focus experiment of segmented mirror*

Bin Li(李斌)[1,2,3,†], Wen-Hao Yu(于文豪)[1,2,3], Mo Chen(陈莫)[1,2,3], Jin-Long Tang(唐金龙)[1,3], and Hao Xian(鲜浩)[1,3,‡]

[1] *Key Laboratory on Adaptive Optics, Chinese Academy of Sciences, Chengdu* 610209, *China*
[2] *University of Chinese Academy of Sciences, Beijing* 100049, *China*
[3] *The Institute of Optics and Electronics, Chinese Academy of Sciences, Chengdu* 610209, *China*

(Received 26 September 2016; revised manuscript received 10 January 2017; published online 20 April 2017)

In this paper, an active optics and co-focus experimental system of segmented mirror is built. Firstly, a support structure of segmented mirror is designed and it is verified by simulation to meet the requirement for the experimental system of segmented mirror. In this system, the large de-focus and tilt/tip errors of the segmented mirror are adjusted by observing the density and contrast of interference fringes based on isoclinic interference theory until the defocus and tilt/tip errors are in the detective range of the Shack–Hartmann. Then, the Shack–Hartmann is used to measure them and they are adjusted by actuators. The actuators are controlled by active optics to realize the closed-loop adjustment and maintenance for fine co-focus of segmented mirror. And the interference fringes are utilized to verify the detective precision of Shack–Hartmann. After the co-focus fine-tuning of the segmented mirror, the tilt/tip residual surface error is better than 0.01λ RMS; the defocus residual surface error is better than 0.01λ RMS.

Keywords: telescope, active or adaptive optics, astronomical, image analysis

PACS: 07.60.–j, 07.60.Ly, 42.68.Wt, 95.55.Cs **DOI:** 10.1088/1674-1056/26/6/060706

1. Introduction

To obtain information about a more distant star, the aperture of the telescope should become larger and larger. At present, there are three design schemes to build a large-aperture telescope, which are lightweight mirror, honeycomb mirror and segmented mirror. But, the aperture of a monoblock telescope cannot be infinitely large due to the limitations of fabrication technology, processing cost, risk factors and so on. To build a more than ten-meter aperture telescope, the technology of segmented mirror should be used, just as adopted in Keck, thirty meter telescope (TMT), and European extremely large telescope (E-ELT).[1–4] But the segmented mirror technology brings about new problems, one of which is that the assembly error of segmented mirror seriously affects the resolution of the telescope. So, only when the segmented mirror is co-focus and co-phasing, can it reach the resolution corresponding to the aperture of segmented mirror.

So far, some relevant work has been done to realize the co-focus and co-phasing of segmented mirror.[5–7] The Keck is the first segmented telescope and it realized co-focus in the visible band and co-phasing in the infrared band in 1998.[8–10] The LAMOST of China also realized the co-focus of segmented mirror in the visible band based on active optics technology.[11] In 2000, Su *et al*. accomplished an indoor co-focus experiment of segmented mirror; three regular hexagon reflecting mirrors, each with 250 mm in diagonal, are used in the experiment. And it realized the co-focus of segmented mirror with an error of co-focus less than $0.035''$.[12] In 2010, Lin *et al*. accomplished a similar experiment. In their experimental system, the segmented mirror consisted of three hexagonal sub-mirrors, each with 300 mm of spacing between sides. And it also realized the co-focus of segmented mirror with an error of co-focus less than $0.02''$.[13] But they did not elaborate how they adjusted the large de-focus and tilt/tip errors into the detective range of Shack–Hartmann, and there was not another equipment to verify the precision of co-focus of segmented mirror in their experimental system either. In 2008, Song He-Lun *et al*. also accomplished an indoor co-focus experiment of segmented mirror based on a high-aperture Michelson interferometer layout.[14] However, it needs an extra light source to detect the tilt/tip error of segmented mirror, which makes the tilt/tip error unable to be detected nor adjusted in real time. For this, we propose that the large tilt/tip and defocus errors are manually adjusted by observing the density and contrast of interference fringes until the defocus and tilt/tip errors are in the detective range of the Shack–Hartmann. Then, the Shack–Hartmann is used to measure the defocus and tilt/tip errors and they are adjusted by the technology of active optics. Finally, the result of fine co-focus of segmented mirror and the detective precision of Shack–Hartmann are verified by the interference fringe. In addition, the support structure of segmented

*Project supported by the National High Technology Research and Development Program of China.
†E-mail: libingioe@126.com
‡Corresponding author. E-mail: xianhao@ioe.ac.cn
© 2017 Chinese Physical Society and IOP Publishing Ltd

mirror is designed and it is verified by the ANSYS simulation and the segmented mirror experiment.

The rest of the paper is organized as follows. In Section 2, we describe the principle of regulation of co-focus. In Section 3, we present the experimental system of co-focus. In Section 4, we describe the method and process of co-focus adjustment of the segmented mirror. The experimental result and its analysis are presented in Section 5 and the conclusions are summarized in Section 6.

2. Principles of regulation of co-focus

2.1. Principles of the Shack–Hartmann wavefront sensor

In the Shack–Hartmann (SH) wavefront sensor, a micro lens array is used to partition and sample the wavefront. As shown in Fig. 1, each micro lens serves as a sub-aperture.

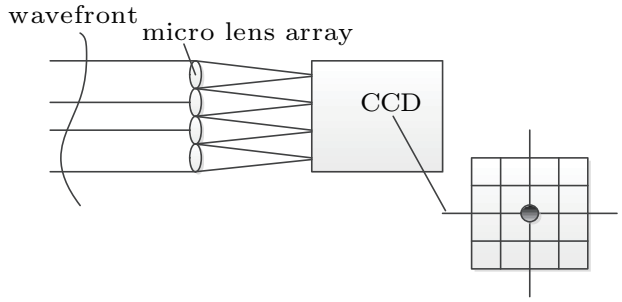


Fig. 1. Principles of Shack–Hartmann wavefront sensor.

When the SH is illuminated by standard parallel light beam, there are array light spots on a charge coupled device (CCD) and the centroid position of each light spot is used as a reference standard. If the wavefront is distorted, the centroid position of the light spot will be offset. Now, we use $(X_{\rm C}, Y_{\rm C})$ to express the CCD centroid position of each light spot and the centroid formula is[15]

$$\begin{cases} X_{\rm C} = \dfrac{\sum X_i I_i}{\sum I_i} = \dfrac{f}{kS}\iint\limits_S \dfrac{\partial \phi(x,y)}{\partial x}\,{\rm d}x{\rm d}y = \dfrac{f}{k}G_X, \\ Y_{\rm C} = \dfrac{\sum Y_i I_i}{\sum I_i} = \dfrac{f}{kS}\iint\limits_S \dfrac{\partial \phi(x,y)}{\partial y}\,{\rm d}x{\rm d}y = \dfrac{f}{k}G_Y, \end{cases} \tag{1}$$

where, (G_X, G_Y) is the mean slope of the sub aperture wavefront, S is the area of the sub aperture, f is the focal length of the micro lens, and k is the wave number. Once the centroid position of the sub aperture spot is obtained, the sub aperture wavefront mean slopes can be calculated from Eq. (1).

2.2. Principles of Zernike modal phase retrieval

The wavefront formula which is described by Zernike polynomial is[15]

$$\varphi(x,y) = a_0 + \sum_{i=1}^{n} a_i Z_i(x,y) + \varepsilon. \tag{2}$$

The relationship between the slope of sub aperture and Zernike polynomial coefficients is as follows:

$$\begin{cases} G_X(i) = \displaystyle\sum_{k=1}^{n} a_k \frac{\iint\limits_{S_i} \dfrac{\partial Z_k(x,y)}{\partial x}\,{\rm d}x{\rm d}y}{S_i} + \varepsilon_x = \sum_{k=1}^{n} a_i Z_{xk}(i) + \varepsilon_x, \\ G_Y(i) = \displaystyle\sum_{k=1}^{n} a_k \frac{\iint\limits_{S_i} \dfrac{\partial Z_k(x,y)}{\partial y}\,{\rm d}x{\rm d}y}{S_i} + \varepsilon_y = \sum_{k=1}^{n} a_i Z_{yk}(i) + \varepsilon_y. \end{cases} \tag{3}$$

The above relationship may be expressed in the form of matrix:

$$\begin{bmatrix} G_X(1) \\ G_Y(1) \\ G_X(2) \\ G_Y(2) \\ \cdots \\ G_X(m) \\ G_Y(m) \end{bmatrix} = \begin{bmatrix} Z_{x1}(1) & Z_{x2}(1) & \cdots & Z_{xn}(1) \\ Z_{y1}(1) & Z_{y2}(1) & \cdots & Z_{yn}(1) \\ Z_{x1}(2) & Z_{x2}(2) & \cdots & Z_{xn}(2) \\ Z_{y1}(2) & Z_{y2}(2) & \cdots & Z_{yn}(2) \\ \cdots & \cdots & \cdots & \cdots \\ Z_{x1}(m) & Z_{x2}(m) & \cdots & Z_{xn}(m) \\ Z_{y1}(m) & Z_{y2}(m) & \cdots & Z_{yn}(m) \end{bmatrix} \begin{bmatrix} a_1 \\ a_2 \\ \vdots \\ a_n \end{bmatrix} + \begin{bmatrix} \varepsilon_{x1} \\ \varepsilon_{y1} \\ \varepsilon_{x2} \\ \varepsilon_{y2} \\ \vdots \\ \varepsilon_{xm} \\ \varepsilon_{ym} \end{bmatrix}. \tag{4}$$

The above matrix form may be further expressed as follows:

$$\boldsymbol{G} = \boldsymbol{Z}\boldsymbol{A} + \boldsymbol{\varepsilon}. \tag{5}$$

So if we acquire the restoration vector $\boldsymbol{Z}$ and the slope vector $\boldsymbol{G}$, Zernike polynomial vector $\boldsymbol{A}$ will be calculated and the wavefront can be recovered.

2.3. Principles of segmented mirror co-focus regulation

When segmented mirror has large tilt/tip and defocus errors, the reference light beam interferes with the light beam which is reflected back by the segmented mirror and the interference fringes are observed in the place of the conjugate surface of the segmented mirror. Then, the large tilt/tip and defocus errors of segmented mirror are manually adjusted by observing the density and contrast of interference fringes until they are in the detective range of the SH wavefront sensor. At this moment, the tilt/tip and defocus errors of segmented mirror are small. Finally, the wavefront is recovered by the SH wavefront sensor; from the wavefront information, the concrete values of tilt/tip and defocus errors can be calculated; the segmented mirror tilt/tip and defocus errors are adjusted by actuators. The sub-aperture arrays corresponding to each sub-mirror of SH wavefront sensor are shown in Fig. 2, from

which we know that each sub-mirror corresponds to twenty sub-apertures; these are enough to calculate the tilt/tip and defocus errors of segmented mirror accurately.

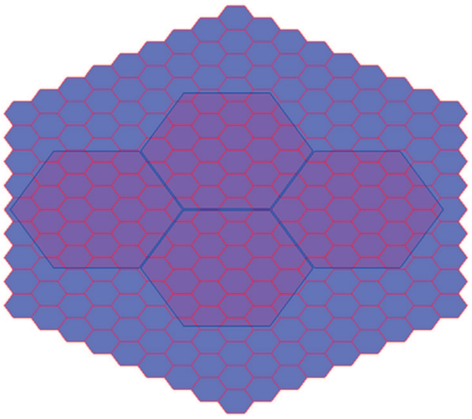


Fig. 2. (color online) Micro lens configurations corresponding to sub-mirrors.

3. Experimental system of co-focus

As shown in Fig. 3, the point light source is collimated by lens 1, the parallel light beam is divided into two parallel light beams by beam splitter 1: one is reflected back by reflectors 1 and 2, and the other is reflected back by the segmented mirror. When the difference in path between two parallel light beams is less than the coherence length of point light source, they will interfere. After that, the parallel light beam is divided into two parallel light beams by beam splitter 2: one passes through lens 3 and enters into the CCD 1 placed at the focus of lens 3; and the other is divided into two parallel light beams by beam splitter 3: one passes through lens 4 and enters into the CCD 2 placed in the conjugate surface of segmented mirror; the other enters into the SH wavefront sensor. When the segmented mirror tilt/tip and defocus errors are adjusted by the actuators, we should keep out of the parallel light beam which is reflected back by reflectors 1 and 2. Figure 4 shows the physical experimental system, in which the segmented mirror is composed of four regular hexagon sub-mirrors; the flat-to-flat length of them is 100 mm, the radii of curvature of them are all 2000 mm, the central thickness values of them are all 15 mm.

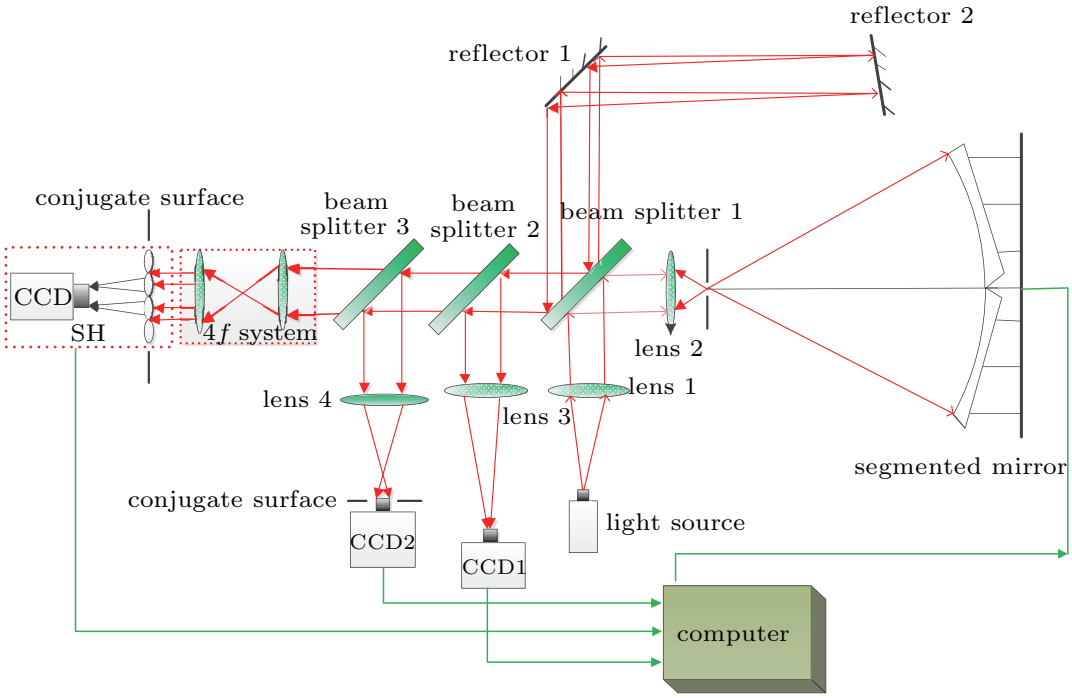


Fig. 3. (color online) Light path of experimental system.

Before the co-focus errors of the segmented mirror are adjusted by actuators, the tilt/tip and defocus errors should be adjusted manually until the tilt/tip and defocus errors are in the detective range of the SH wavefront sensor.

The size of clear aperture of the SH wavefront sensor is 15.2 mm×17.6 mm; the aperture arrays of the SH wavefront sensor are 17×17 regular hexagons of flat-to-flat length 1.034 mm; the focal length of the micro lens is 100 mm. The focal lengths of lenses 1, 2, and 4 are all 100 mm, the focal length of lens 3 is 400 mm. The resolutions of CCD 1 and CCD 2 are both 582×776, and the size of pixel of them is 8.3 μm; the resolution of CCD of the SH wavefront sensor is 3296×2472, the size of pixel of it is 5.5 μm; the metrical range of the SH wavefront sensor is 0.01 rad.

As shown in Fig. 5, the regulation mechanism of segmented mirror can be divided into two levels: one is coarse adjustment and the other is fine adjustment. The coarse adjustment is composed of three precision adjusting screws and

it realizes the millimeter level range and the regulation of micrometer level adjustment. The fine adjustment is composed of three piezoelectric ceramic actuators and it realizes the range of 100 μm and the regulation of 2-nm adjustment. The support structure of the segmented mirror can eliminate the influence on the surface of the sub-mirror, which is caused by gravity. As shown in Fig. 6, when the sub-mirror is subjected to only gravity force, the peak value (PV) of the sub-mirror is 2.3 nm; the root-mean-square (RMS) of the sub-mirror is 0.5 nm. As shown in Fig. 7, when each actuator of the sub-mirror is subjected to a 6.5 N force, figure 7(a) shows that the piston displacement of the sub-mirror is 80 μm, figure 7(b) shows the PV of the sub-mirror is 58 nm and the RMS of the sub-mirror is 12.8 nm.

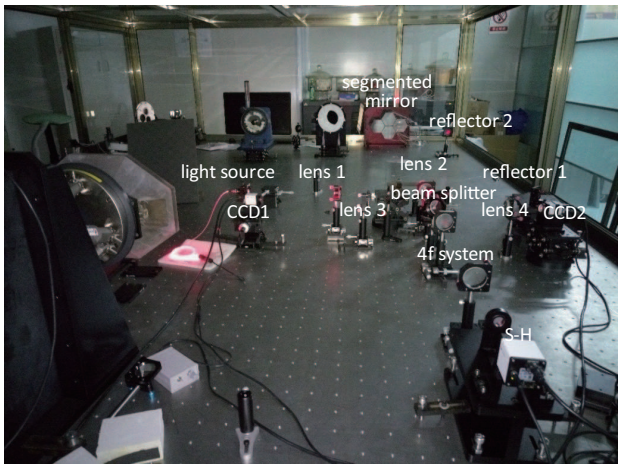


Fig. 4. (color online) Physical experimental system.

From the ANSYS simulation, we know that the surface error of the sub-mirror changes very little in the presence of only gravity. When the sub-mirror has a large displacement which is caused by actuators, the surface error of the sub-mirror is also small. So the support structure of the segmented mirror meets the requirement for experiment.

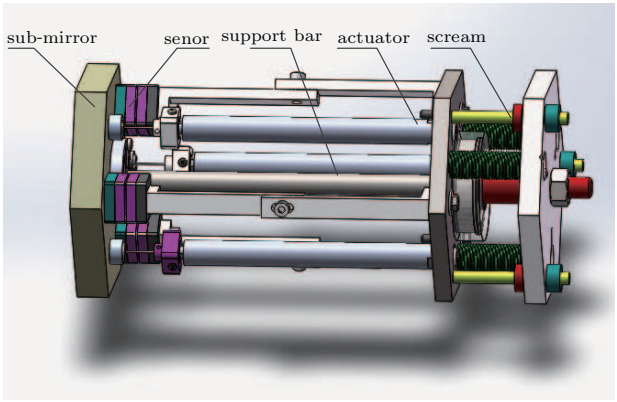


Fig. 5. (color online) Support structure of segmented mirror.

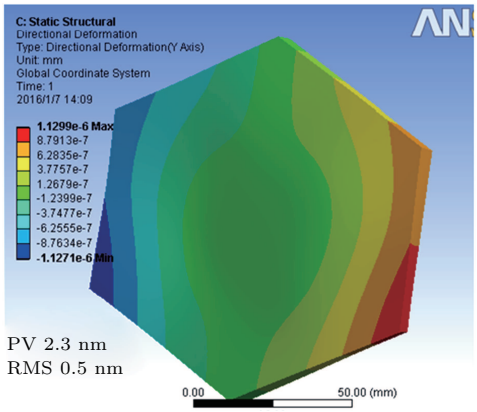


Fig. 6. (color online) ANSYS simulation in the presence of only gravity force.

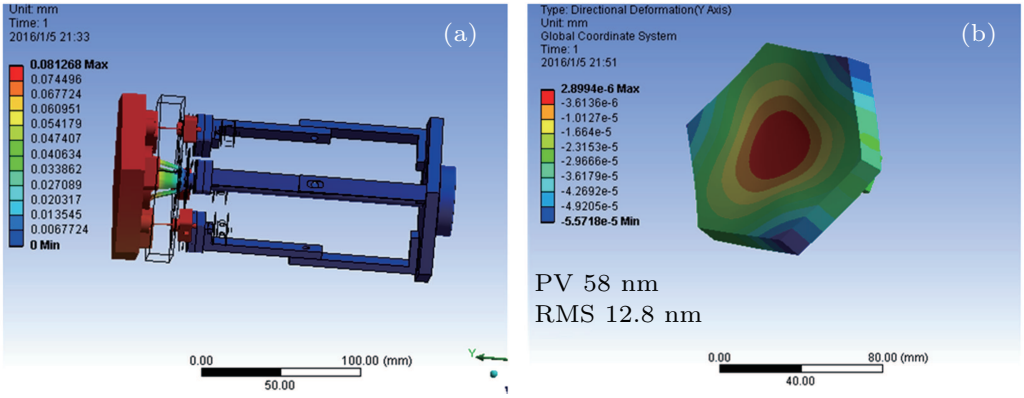


Fig. 7. (color online) ANSYS simulation, when the actuators are subjected to force. (a) The ANSYS simulation displacement of sub-mirror when all actuators are under the action of a force of 6.5 N; (b) the ANSYS simulation surface errors of sub-mirror when all actuators are acted by a force of 6.5 N.

4. Method and process of co-focus adjustment of segmented mirror

Before using the SH wavefront sensor, the spherical reflector whose radius of curvature is 200 millimeters is used as the reference mirror and its surface error is less than 0.01λ. Then, the SH wavefront sensor is calibrated to eliminate its alignment error. Because of the uneven surface of the beam splitter, there is a stray light beam entering into the SH wave-

front sensor, thereby leading to inaccurate results measured by the SH wavefront sensor. For this, a proper threshold is set to eliminate the influence of the stray light beam. Moreover, the background value of the SH camera is subtracted to eliminate the influence of the background noise of the SH camera.

After the SH wavefront sensor is calibrated, the tilt/tip and defocus errors of each sub-mirror are adjusted manually until the light beam enters into the CCD2. The data of Fig. 8 are obtained from CCD2. When the interference fringes appear as those indicated in Fig. 8(a), we continue to adjust the defocus and tilt/tip errors until the density of interference fringes is small and the contrast of interference fringes is as good as that in Fig. 8(b).

When the tilt/tip and defocus errors are in the detecting range of the SH wavefront sensor, the error which is measured by SH is adjusted by actuators.

As shown in Fig. 9, when the tilt/tip and defocus errors of the segmented mirror are changed, the errors will be measured by the SH wavefront sensor, and they will be adjusted by actuators.

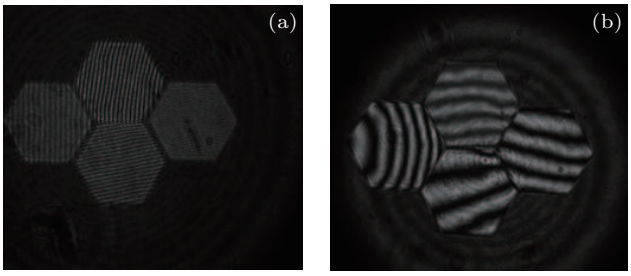


Fig. 8. (a) Interference fringes when the segmented mirror has a large tilt/tip error; (b) the interference fringes when the segmented mirror has a small tilt/tip error.

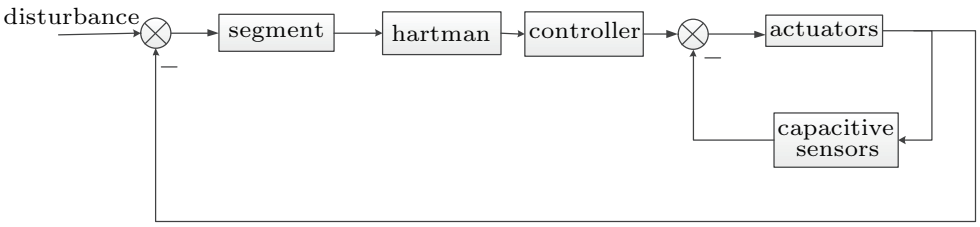


Fig. 9. Segmented mirror control flow chart.

The following equation is the control equation of active optics:

$$\boldsymbol{S} = \boldsymbol{A}_1 \boldsymbol{P}, \tag{6}$$

where $\boldsymbol{S}$ is the value vector of three capacitive sensors; $\boldsymbol{P}$ is the value vector of three actuators; $\boldsymbol{A}_1$ is the transfer vector from the values of actuators to the values of capacitive sensors.

$$\boldsymbol{P} = \boldsymbol{A}_2 \boldsymbol{H}, \tag{7}$$

where $\boldsymbol{A}_2$ is the transfer vector from segmented mirror tilt/tip error values to actuator values and $\boldsymbol{H}$ is the segmented mirror tilt/tip error value vector.

From Fig. 10(a), we can calculate $\boldsymbol{A}_1$ and $\boldsymbol{A}_2$:

$$\boldsymbol{A}_1 = \frac{1}{3} * \begin{bmatrix} 2 & -1 & 2 \\ 2 & 2 & -1 \\ -1 & 2 & 2 \end{bmatrix},$$

$$\boldsymbol{A}_2 = \begin{bmatrix} 0 & -a \\ (\sqrt{3}/2)a & a/2 \\ -(\sqrt{3}/2)a & a/2 \end{bmatrix}.$$

The data of Figs. 10(b) and 10(c) are obtained from the SH camera. As shown in Fig. 10(b), when the segmented mirror has tilt/tip and defocus errors, the corresponding spots of the SH wavefront sensor will be offset. According to the formula (1), the restoration vector $\boldsymbol{G}$ can be calculated. According to formula (3), the restoration vector $\boldsymbol{Z}$ can be calculated. So, the tilt/tip and defocus errors of each sub-mirror can be calculated from formulas (4) and (5), and the values of capacitive sensors can be calculated from formulas (6) and (7). Then each actuator is controlled by active optics until the values of capacitive sensors are consistent with the calculated values. From Fig. 10(c), we know that all of the spots are in the center of the sub aperture after fine co-focus of the segmented mirror.

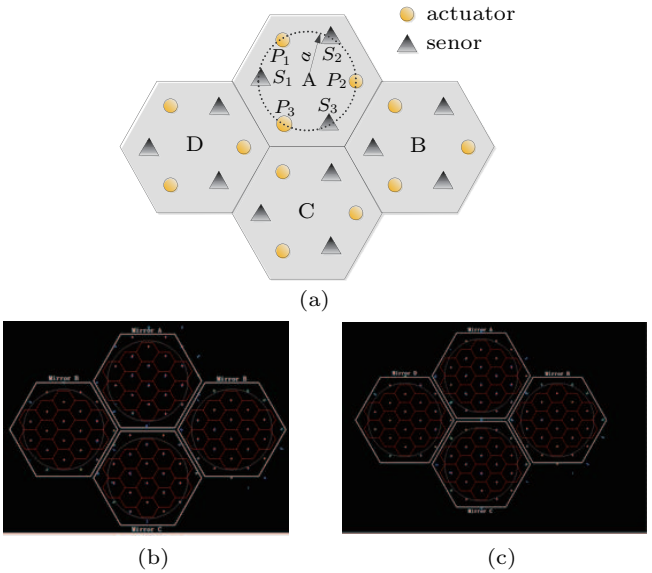


Fig. 10. (color online) (a) Configurations of actuators and capacitive sensors; (b) the spots of SH wavefront sensor before adjusting the segmented mirror co-focus; (c) the spots of SH wavefront sensor after adjusting the segmented mirror co-focus adjustment.

5. Experimental results and analysis

5.1. Judging the quality of co-focus based on far field spot

According to far field diffraction theory, when the segmented mirror is absolute co-focused, the energy of the far field spot is the sum of energies of all the sub-mirrors. So, the ratio between the max value of energy of the far field spot of the segmented mirror co-focus and the sum of the max values of the energy of the far field spot of all the sub-mirrors can be used to judge the quality of segmented mirror co-focus.

We define

$$\mathrm{SR} = \frac{\text{the max value of energy of far field spot of segmented mirror co-focus}}{\text{the sum of the max value of energy of far field spot of all the sub-mirrors}}. \tag{8}$$

Figure 11 shows the practical far field spots of segmented mirror, and it is obtained from CCD 1. From Fig. 11(a), we know that the energy intensity of the far field spot of each sub-mirror is different. It is because the center of the light source does not coincide with the center of the segmented mirror. When the segmented mirror is absolutely co-focused, the SR is 1. As shown in Fig. 11(d1), when the segmented mirror is fine co-focused, the SR is 0.96, which is very close to the theoretical value. Therefore, the quality of the segmented mirror co-focus is perfect.

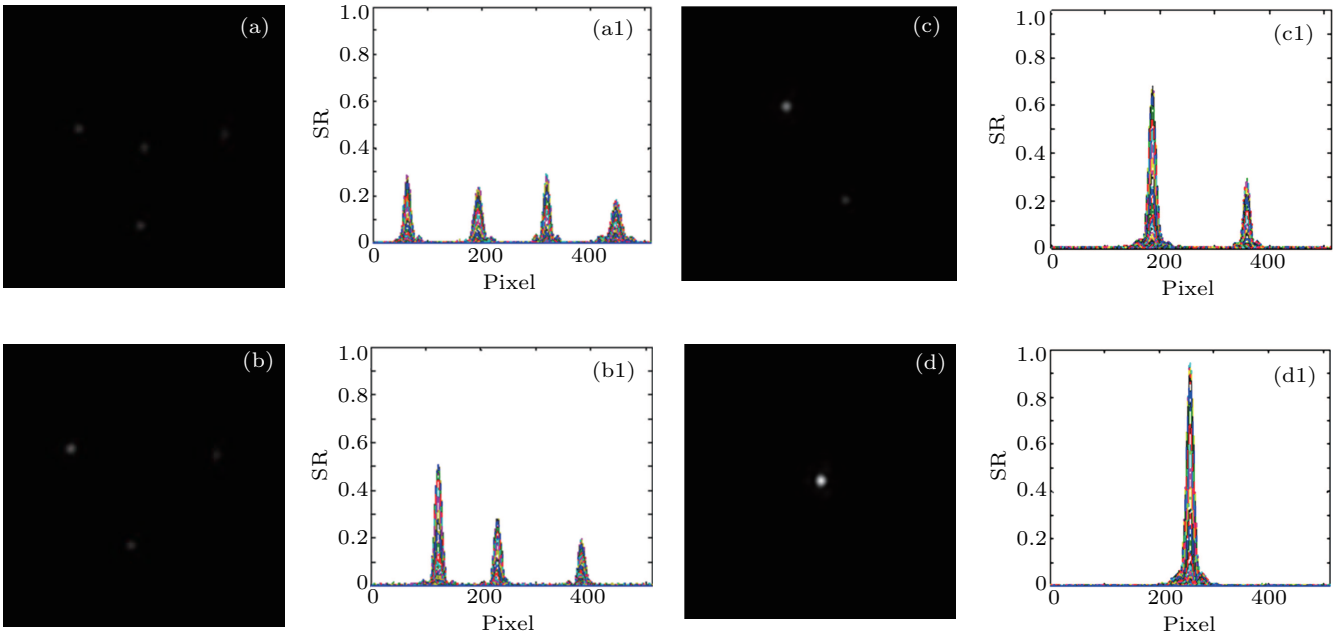


Fig. 11. (color online) (a) Far field spot with segmented mirror de-focused and (a1) the intensity of far field spot with segmented mirror de-focused; (b) the far field spot with 2 sub-mirrors co-focused and (b1) the intensity of far field spot with 2 sub-mirrors co-focused; (c) the far field spot with 3 sub-mirrors co-focused and (c1) the intensity of far field spot with 2 sub-mirrors co-focused; (d) the far field spot with 4 sub-mirrors co-focused and (d1) the intensity of far field spot with 4 sub-mirrors co-focused.

The metrical precision of SH wavefront sensor is about 1/10 pixel, as the size of pixel of the CCD of SH is 5.5 μm and the focal length of micro lens is 100 mm, so the precision of tilt/tip error which is measured by the SH wavefront sensor is $1/20 * 5.5/100 \times 3.6 \times 57.3 = 0.5''$. As the focal length of lens 2 is 100 mm, the radius of curvature of segmented mirror is 2000 mm, so the tilt/tip error of the segmented mirror is $0.25'' \times 100/2000/2 = 0.025''$, and it can be transformed into the surface error which is 0.01λ RMS. The defocus error which is measured by the SH wavefront sensor is less than 0.01λ RMS, and it can be transformed into the axial residual error which is less than 50 μm.

5.2. Comparison and analysis of figure based on isoclinic interference theory

Based on isoclinic interference theory, when the surface error of the segmented mirror is larger than 0.25λ, the interference fringes will appear and the number of interference fringes increases in proportion to the tilt/tip error. So, the tilt/tip error can be calculated accurately by the number of interference fringes. When the segmented mirror is co-focused, the reflector 2 is adjusted to make calibration light beam have tilt error; the tilt error which is calculated by the number of interference fringes compares with the metrical result of the SH wavefront sensor.

The data of Fig. 12 is obtained from CCD2. As shown in Fig. 12, when the calibration light beam has a tilt error, the

interference fringes will appear. From Fig. 12(a), we can obtain a distance of adjacent interference fringes of 34 pixels, and a flat-to-flat distance of sub-mirror of 176 pixels. So, the tilt error is $\lambda/2*34/176/2 = 1.29\lambda$, and the tilt error which is measured by the SH wavefront sensor is 1.28λ RMS. The result indicates that the metrical precision of the SH wavefront sensor is less than 0.01λ RMS. As shown in Fig. 12(b), there are not whole interference fringes, which means that the tilt/tip error is less than 0.25λ.

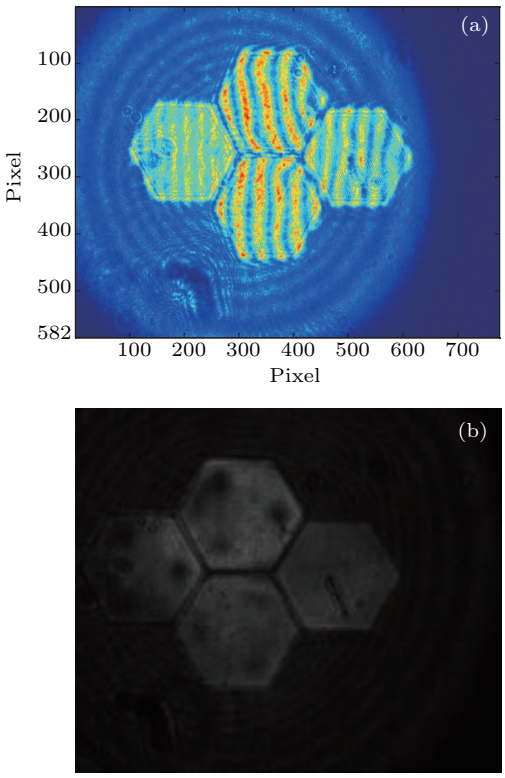


Fig. 12. (color online) (a) Interference fringes when the calibration light beam has a tilt error; (b) the interference fringes when the segmented mirror has fine co-focus.

6. Conclusions and perspectives

The research builds an active optics and co-focus experiment system of segmented mirror, in which system the support structure of the segmented mirror is designed and it is verified by ANSYS simulation. In experiment, the large defocus and tilt/tip errors of segmented mirror are adjusted manually; the small defocus and tilt/tip errors are adjusted by actuators, and the actuators are controlled by active optics. After using the method proposed in the paper, the tilt/tip residual surface error is better than 0.01λ RMS, and it can be transformed into the angle of inclination of the segmented mirror, which is less than $0.025''$; the defocus residual error is better than 0.01λ RMS, and it can be transformed into an axial residual error, which is less than 50 μm. It demonstrates that the method which is proposed in the paper can realize the adjustment and maintenance of fine co-focus of segmented mirror, and the method can make the tilt/tip error be detected and adjusted in real time.

References

[1] Jared R C, Arthur A, Andreae S, Biocca A K, Cohen R W, Fuertes J M, Franck J, Gabor G, Lacer J L and Mast T S 1990 *Proc. SPIE* **19** 1038
[2] Chanan G A, Nelson J E and Mast T S 1986 *Proc. SPIE* **10** 1741
[3] Bonnet H, Esselborn M, Kornweibel N and Dierickx P 2014 *Proc. SPIE* **9145** 91451U
[4] Troy M, Chanan G A, Give'On A, Roberts J, Rodgers J M, Scherr L M and Seo B J 2008 *Proc. SPIE* **7012** 70120Y
[5] Luo Q, Huang L H, Gu N T and Rao C H 2012 *Chin. Phys. B* **21** 094201
[6] Luo Q, Huang L H, Gu N T, Li F and Rao C H 2012 *Acta Phys. Sin.* **61** 069501 (in Chinese)
[7] Yan Z J, Chen X Y, Yang P Q, Zhou D, Zheng LX and Zhu N H 2015 *Acta Phys. Sin.* **64** 149501 (in Chinese)
[8] Chanan G A, Mast T S, Nelson J E, Cohen R W and Wizinowich P L 1994 *Proc. SPIE* **2199** 622
[9] Weisskopf M C, Aldcroft T L, Bautz M, Cameron R A, Dewey D, Drake J J, Grant C E, Marshall H L and Murray S S 2005 *Experimental Astronomy* **16** 1
[10] Mast T S and Nelson J E 1982 *Appl. Opt.* **21** 2631
[11] Su D Q and Cui X Q 1999 *Process in Astronomy* **17** 1
[12] Su D Q, Zou W Y, Zhang Z C, Qu Y G, Yang S Y, Wang L J and Rao Y M 2000 *Proc. SPIE* **4003** 417
[13] Lin X D, Chen T, Wang J L, Yang F, Zhang J X, Ming M, Zhang L M, Chen B G, Li Z H and Wang F G 2010 *Opt. & Precision Engineering* **18** 563
[14] Song H L, Jiang W H, Xian H and Li H Q 2008 *Chinese Journal of Lasers* **35** 749
[15] Jiang W H and Li H G 1990 *Proc. SPIE* **1271** 82